Digest Journal of Nanomaterials and Biostructures Vol. 19, No. 4, October-December 2024, p. 1817-1823

Synthesis and analysis of bismuth oxychloride and bismuth tungstate using cyclic microwave irradiation method for photocatalytic applications

S. Wannapop [a,*], A. Saisata [a], N. Bamrungpitak [a], Y. Chuminjak [b], A. Somdee [a]
[a] *Faculty of Science, Energy and Environment, King Mongkut's University of Technology North Bangkok, Rayong Campus, Rayong 21120, Thailand*
[b] *Energy Storage Technology Research Team (ESTT), Energy Innovation Research Group (EIRG), National Energy Technology Center (ENTEC), National Science and Technology Development Agency (NSTDA), 111 Thailand Science Park, Thanon Phahonyothin, Tambon Khlong Nueng, Amphoe Khlong Luang, Pathum Thani 12120, Thailand*

The BiOCl and Bi_2WO_6 successfully used the cyclic microwave method at 450 W. The structure, morphology, and optical properties were analyzed using X-ray diffraction (XRD), electron microscopy (SEM), transmission electron microscopy (TEM), and UV-visible spectrophotometer. The impact of dye treatment from photocatalytic synthesis, with and without pH adjustment, was also examined. It was discovered that the pH adjustment of the Bi_2WO_6 photocatalyst improved the treatment of MO dyes to 91% removal after 80 minutes. Additionally, the ability of the photocatalyst to treat other dyes, such as rhodamine B (RhB) and methylene Blue (MB), was evaluated.

(Received September 20, 2024; Accepted November 27, 2024)

Keywords: BiOCl, Bi_2WO_6, Photocatalysis, SEM, TEM

1. Introduction

The rise of industry worldwide and the subsequent growth of industrial factories have led to increased water usage and the generation of more industrial wastewater. The textile and dyeing industry, in particular, has experienced rapid economic growth due to the essential role of textiles in human life. However, the production processes in this industry require the use of large quantities of chemicals and dyes, resulting in wastewater with high levels of contamination. If this wastewater is not treated before being discharged into natural water sources, it can severely impact living organisms and the environment, potentially leading to the destruction of natural water source ecosystems.

While various technologies, such as adsorption with activated carbon, membrane filtration, coagulation-flocculation, chemical oxidation, and ozone oxidation, are currently used for wastewater treatment, these methods often come with high costs and leave residual sludge after treatment [1–3]. In contrast, photocatalytic processes for treating wastewater, particularly from dyeing processes, offer a promising solution. These processes can effectively remove dyes without leaving residual sludge or contaminants, providing a more sustainable and cost-effective approach to wastewater treatment [4].

Photocatalytic processes typically utilize semiconductor materials such as titanium dioxide (TiO2) and zinc oxide (ZnO) [5–6]. However, TiO_2 and ZnO require ultraviolet (UV) light with wavelengths of approximately 280 – 380 nanometers in order to activate and generate electrons and holes for the reaction [7]. Since only about 5 percent of sunlight is UV light, this limits the full utilization of solar energy. Given that visible light, which has a wavelength of 400 – 700 nanometers, is more abundant, researchers worldwide are developing new semiconductor materials that can more effectively absorb light across the visible spectrum. Researchers are currently seeking

* Corresponding author: surangkana.w@sciee.kmutnb.ac.th
https://doi.org/10.15251/DJNB.2024.194.1817

semiconductors that can enhance the efficiency of pollutant treatment by maximizing the use of natural energy sources.

Recently, bismuth-based photocatalysts such as BiOCl [8], BiOBr [9], Ag@Ag_2O-$PbBiO_2Br$ [10], Zr–BiOI/GO composite [11], Bi_2S_3/BiOI [12], sm-$BiVO_4$ [13], and Bi_2WO_6/TiS_2 [14] have become popular research topics.

Among bismuth-based photocatalysts, bismuth oxyhalides (BiOX, where X = Cl, Br, or I) stand out as promising candidates [15]. These materials possess a unique layered structure that induces atomic polarization, creating an electrostatic field that significantly prolongs the lifespan of light-induced charges. This property helps reduce the recombination of charge carriers, a crucial factor in enhancing photocatalytic efficiency. Additionally, BiOX materials are chemically inert, non-toxic, and resistant to corrosion in aqueous environments, further increasing their appeal. Composed of various compounds sensitive to visible light, these materials hold great potential in photocatalysis.

Bismuth-based metal oxides like Bi_2MO_6 (M = W, Mo, Cr) are also interesting candidates for bismuth-based photocatalysis [16]. These materials have garnered significant attention in photocatalysis due to their unique structural and electronic properties. These materials exhibit good photocatalytic properties, partly because of their narrow band gap energies, which are typically less than 3.0 eV. The electronic structure of these bismuth oxides is characterized by a valence band comprised of hybrid orbitals of bismuth 6s and oxygen 2p.

Based on the aforementioned properties, this research focuses on developing catalysts from bismuth-based metal oxides and bismuth oxyhalides groups. Specifically, bismuth tungstate (Bi_2WO_6) and bismuth oxychloride (BiOCl) were chosen and synthesized using the cyclic microwave irradiation method. The study investigates the effects of pH adjustment and non-adjustment and evaluates the catalysts' effectiveness in treating the dyes MO, RhB, and MB. It was found that bismuth tungstate demonstrated the best dye treatment performance.

2. Experimental

2.1. Synthesis of non-pH-adjusted and pH-adjusted bismuth oxychloride

To synthesize bismuth oxychloride (BiOCl) without pH adjustment, 1.485 g of $Bi(NO_3)_3$•$5H_2O$ was dissolved in 60 mL of deionized (DI) water in a rose-shaped bottle. Then, 6 ml of HCl was added to the solution, and it was stirred vigorously for 10 minutes. The mixture was then subjected to cyclic microwave irradiation at 450 watts for two cycles (10 minutes on, 1 minute off). After synthesis, the sample was cooled to room temperature, then centrifuged and washed using DI water, followed by ethanol. The sample was subsequently dried in an oven at 60 °C for 24 hours and annealed at 400 °C for 30 minutes. This sample was labeled BC-N.

The synthesis of bismuth oxychloride (BiOCl) with pH adjustment followed a similar procedure, with the pH adjusted to 6 using 1 M HNO_3 and NaOH. This sample was labeled BC-pH6.

2.2. Synthesis of non-pH-adjusted and pH-adjusted bismuth tungstate

Bismuth tungsten (Bi_2WO_6) synthesis involved dissolving 1.486 g of $Bi(NO_3)_3$•$5H_2O$ and 1.01 g of Na_2WO_4•$2H_2O$ in 30 ml of DI water. The solution was mixed and stirred for 30 minutes to synthesize the compound. The pH was either adjusted or left unadjusted, using the codes BW-N for no adjustment and BW-pH6 for adjustment, following the same method as for BiOCl.

The samples were analyzed using X-ray diffraction (XRD, Bruker AXS D8 eco), transmission electron microscopy (TEM, JEOL, JEM-2010), and scanning electron microscopy (SEM, JEOL, JSM 6335F). The photocatalytic properties of the products were assessed by exposing MO solutions to a xenon lamp with consistent light intensity. For the photocatalytic activity tests, 0.2 g of catalyst was dispersed in 200 ml of 1×10^{-5} M MO aqueous solutions and kept in the dark for 30 minutes under magnetic stirring. During the photocatalytic testing, a 5 ml solution sample was collected and centrifuged every 10 minutes. The residual MO concentration was measured at the 465 nm wavelength peak using UV-Visible spectrophotometry (Shimadzu UV-2600). Similar methods were applied for MB and RhB dyes, with concentrations measured at 664 nm and 554 nm, respectively.

3. Results and discussions

Fig. 1a shows the XRD patterns of BC-N and BC-pH6. The BC-N sample aligns with the standard peaks on JCPDS card no. 06-0249, corresponding to oriented BiOCl in a tetragonal structure. The X-ray diffraction pattern shows 19 peaks for bismuth oxychloride at 2θ angles of 11.82°, 25.30°, 27.40°, 36.10°, 36.90°, 37.80°, 38.60°, 48.10°, 53.90°, 55.10°, 56.60°, 62.70°, 68.70°, 70.30°, and 75.10°. These peaks correspond to the planes (001), (002), (101), (110), (102), (111), (003), (112), (200), (201), (113), (202), (211), (104), (212), (114), (220), (214), and (310), respectively.

For the BC-pH6 sample, after adjusting the pH to 6, it was discovered that BiOCl also exhibited a tetragonal structure. The X-ray diffraction pattern revealed 20 peaks for bismuth oxychloride at 2θ at angles of 11.93°, 24.10°, 25.90°, 32.50°, 33.40°, 33.40°, 34.80°, 36.50°, 40.90°, 46.60°, 48.30°, 49.70°, 54.10°, 55.10°, 58.60°, 60.50°, 68.10°, 74.10°, 74.90°, and 74.10°. These peaks correspond to the planes (001), (002), (101), (110), (102), (111), (003), (112), (200), (201), (113), (202), (211), (104), (212), (114), (220), (301), (214), and (310), respectively, as shown in Fig. 1a, and also match the standard peaks on JCPDS card no. 06-0249.

Fig. 1b presents the XRD analysis of the BW-pH sample, synthesized using the cyclic-microwave method. The analysis revealed that Bi_2WO_6 has a tetragonal structure, with 9 distinct peaks at 2θ angles of 28.60°, 33.10°, 36.20°, 47.30°, 56.00°, 58.40°, 68.40°, 76.10°, and 78.30°. These peaks correspond to the planes (103), (200), (202), (220), (303), (107), (400), (109), and (307), respectively, and match the standard peaks on JCPDS card no. 26-1044. When comparing the XRD peaks in Fig. 1b, it can be seen that the crystallinity of the BW-pH6 sample is higher than that of the sample without pH adjustment, and the XRD peak pattern shows without pH adjustment, it is a broad peak, indicating a small crystal size. [17].

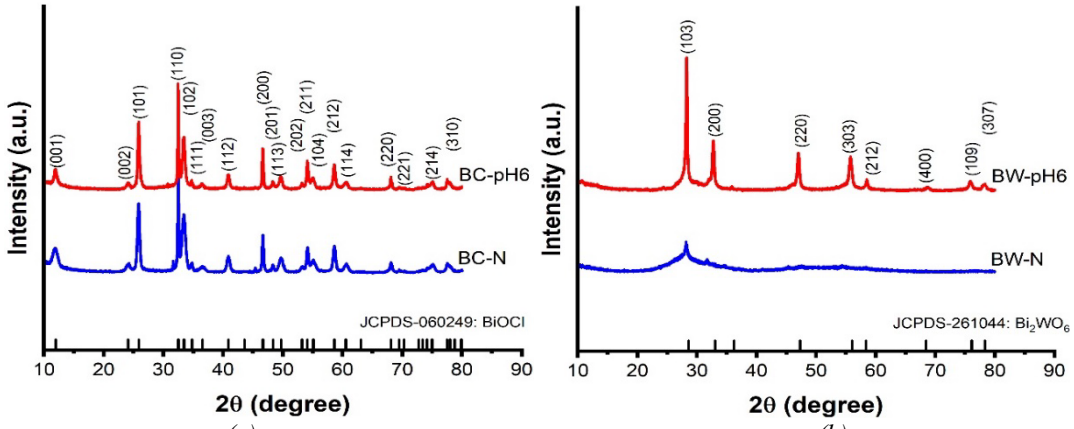

Fig. 1. (a) XRD patterns of BC-N (blue), and BC-pH6 (red); (b) XRD patterns of BW-N (blue), and BW-pH6 (red).

Fig. 2 shows SEM images of BC-N, BC-pH6, BW-N, and BW-pH6. The SEM images reveal that Bi_2WO_6 exists as particles, and after pH adjustment, the particle size of Bi_2WO_6 decreases. Both BC-N and BC-pH6 nanoparticles have a nanoplate structure. A comparison between BiOCl before and after pH adjustment revealed that the pH-adjusted BiOCl has larger sheet sizes compared to the non-adjusted BiOCl.

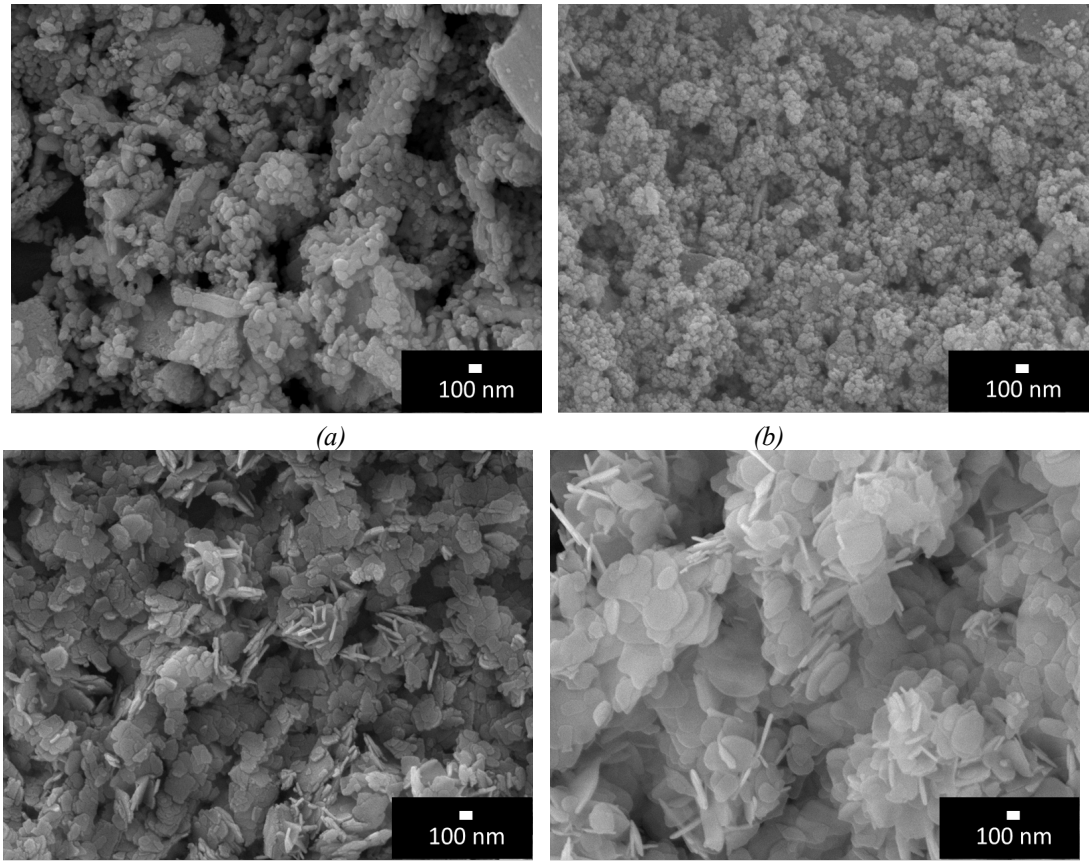

Fig. 2. SEM images of (a) BW-N, (b) BW-pH6, (c) BC-N, and (d) BC-pH6.

In Fig. 3a, the TEM image of BW-pH6 shows nanoparticles with particle sizes ranging from approximately 20 – 50 nm. The high-resolution transmission electron microscopy (HRTEM) image (Fig. 3b) of BW-pH6 displays a lattice fringe spacing of 0.312 nm, corresponding to the (103) planes of tetragonal Bi_2WO_6.

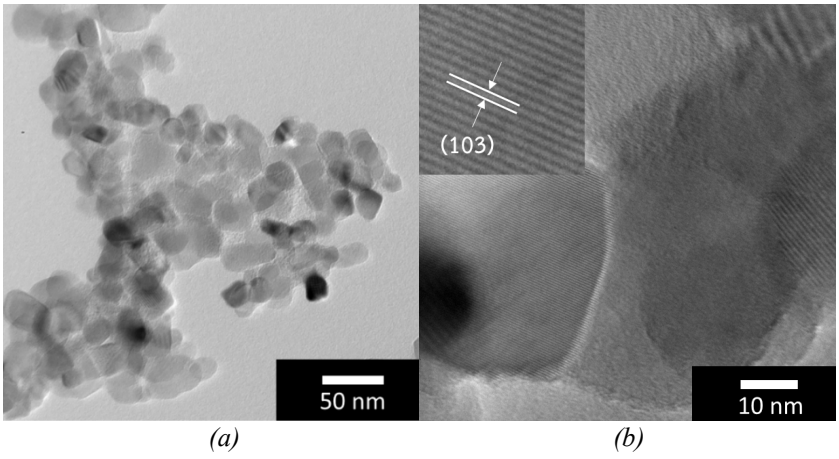

Fig. 3. (a) TEM images of BW-pH6; (b) high-resolution TEM of BW-pH6.

The optical properties of BC-N, BC-pH6, BW-N, and BW-pH6 were characterized by UV-visible spectroscopy (Fig. 4). In this research, BW-pH6 demonstrates excellent absorption compared to the other samples. The calculated bandgap energies for BC-N, BC-pH6, BW-N, and BW-pH6 were 3.50, 3.49, 3.22, and 3.18 eV, respectively.

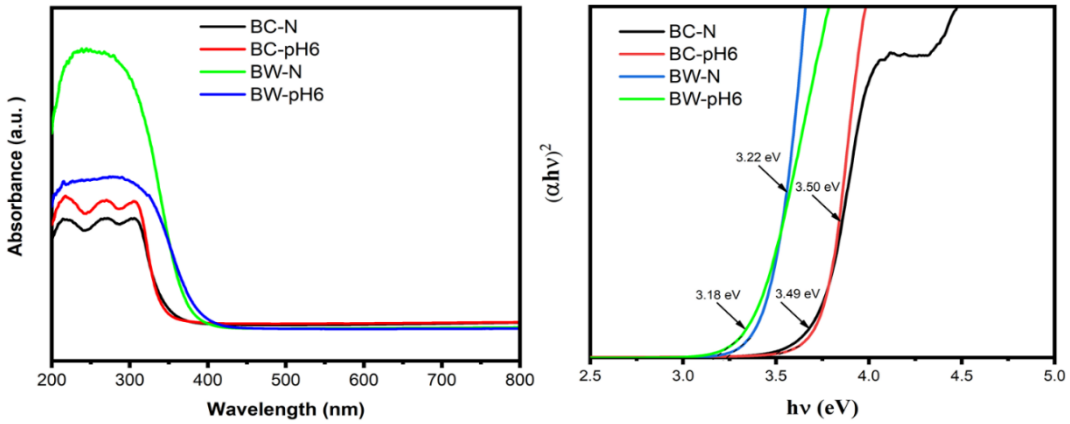

Fig. 4(a) UV-Vis spectra, and (b) band gap energy of BC-N, BC-pH6, BW-N, and BW-pH6.

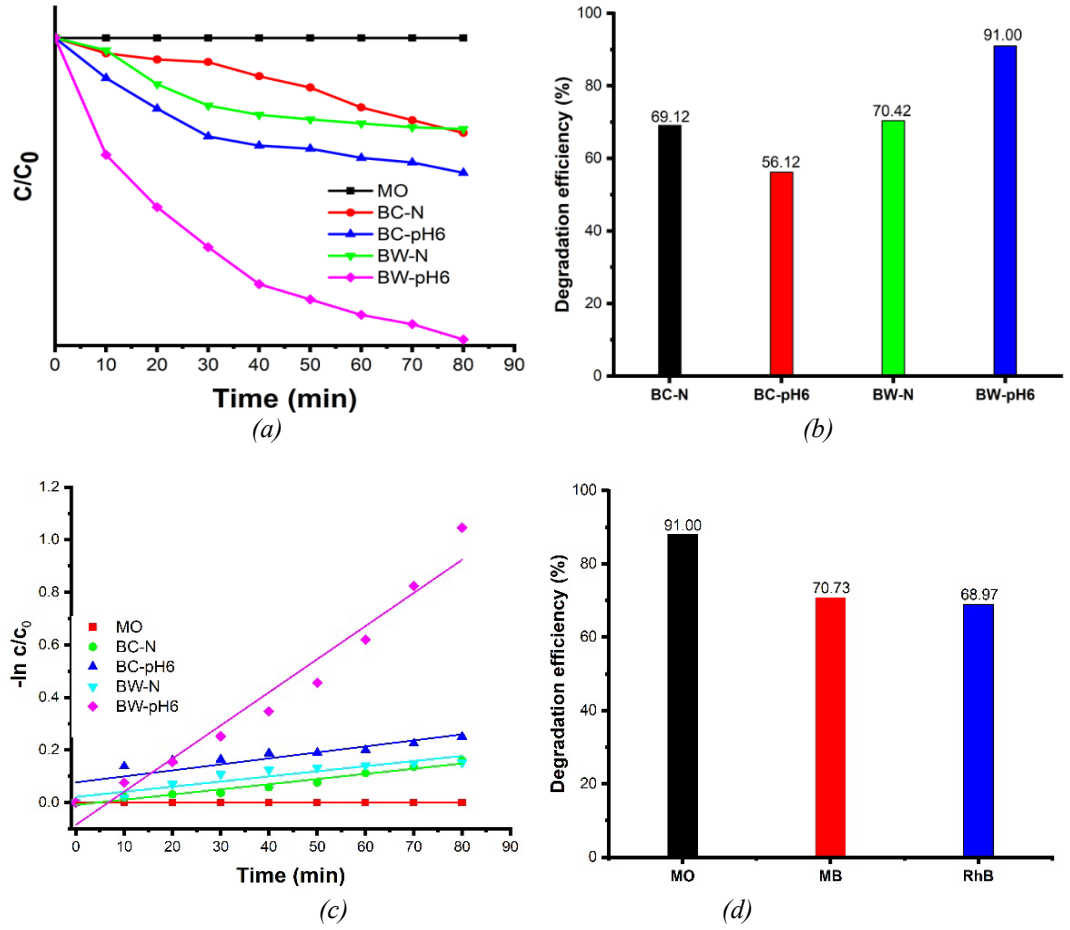

Fig. 5. (a) C/C_o vs. time, (b) Degradation efficiency using MO, (c) pseudo-first-order plot for photodegradation of BC-N, BC-pH6, BW-N, and BW-pH6, and (d) degradation efficiency of BW-pH6 difference dye.

Fig. 5c plots $\ln(C/C_0)$ against different treatment times for the catalysts BC-N, BC-pH6, BW-N, and BW-pH6, and their corresponding kinetic rates were found to be 0.00197 min^{-1}, 0.00228 min^{-1}, 0.00195 min^{-1}, and 0.01878 min^{-1}, respectively. Again, BW-pH6 performed well and exhibited the highest treatment capability after 80 minutes. Initial experiments showed that the BW-pH6 synthesized using cyclic microwave irradiation was the most effective in treating MO dye. As a result, BW-pH6 was further evaluated for its efficacy in treating MB and RhB dyes, and it demonstrated treatment efficiencies of 70.73% and 68.97%, respectively.

4. Conclusions

This research involved synthesizing bismuth oxychloride and bismuth tungstate using the cyclic microwave irradiation method to enhance the performance of the catalysts in treating dyes. Evaluating the synthesized catalysts with methyl orange (MO) dye under xenon light revealed that pH-adjusted bismuth tungstate (BW-pH6) exhibited superior treatment efficiency compared to other catalysts. Furthermore, this catalyst was also effective in treating methylene blue (MB) and rhodamine B (RhB) dyes.

Acknowledgments

This research was funded by King Mongkut's University of Technology, North Bangkok. Contract no. KMUTNB-66-KNOW-08.

References

[1] F. E. Titchou, H. Zazou, H. Afanga, J. El Gaayda, R. A. Akbour, P. V. Nideesh, M. Hamdani, Chemical Engineering and Processing – Process Intensification **169**, 108631 (2021); https://doi.org/10.1016/j.cep.2021.108631
[2] Y. Yue, X. Yue, X. Tang, L. Han, J. Wang, S. Wang, C. Du, Heliyon, **10**(10), e30817 (2024); https://doi.org/10.1016/j.heliyon.2024.e30817
[3] R. M. El-taweel, N. Mohamed, K. A. Alrefaey, S. Husien, A. B. Abdel-Aziz, A. I. Salim, N. G. Mostafa, L. A. Said, I. S. Fahim, A. G. Radwan, Current Research in Green and Sustainable Chemistry **6**, 100358 (2023); https://doi.org/10.1016/j.crgsc.2023.100358
[4] W. Mao, X. Shen, L. Zhang, Y. Liu, Z. Liu, Y. Guan, Frontiers of Environmental Science & Engineering **18**, 86 (2024); https://doi.org/10.1007/s11783-024-1846-x
[5] T. Z. Liza, Md. M. H. Tusher, F. Anwar, M. F. Monika, K. F. Amin, F. N. U. Asrafuzzaman, Results in Materials **22**, 100559 (2024); https://doi.org/10.1016/j.rinma.2024.100559
[6] J. Liu, Q. Xia, C. Chen, Vacuum **228**, 113528 (2024); https://doi.org/10.1016/j.vacuum.2024.113528
[7] A. S. Yusuff, L. T. Popoola, A. O. Gbadamosi, A. I. Igbaf, Materials Today Communications **38**, 107999 (2024); https://doi.org/10.1016/j.mtcomm.2023.107999
[8] X. Miao, F. Ma, F. Qian, H. Zhao, X. Li, Y. Zhou, Inorganic Chemistry Communications **168**, 112948 (2024); https://doi.org/10.1016/j.inoche.2024.112948
[9] S. Li, C. Deng, P. G. Karmaker, K. Yang, J. Wang, W. Liu, X. Yang, Materials Research Bulletin **178**, 112895 (2024); https://doi.org/10.1016/j.materresbull.2024.112895
[10] A. Nazir, A. T. Rasool, P. Huo, M. S. Jagirani, Journal of Water Process Engineering **59**, 105033 (2024); https://doi.org/10.1016/j.jwpe.2024.105033
[11] L. Wang, R. Gao, J. He, J. Huang, H. Chen, W. Yao, X. Cai, Journal of Solid State Chemistry **332**, 124586 (2024); https://doi.org/10.1016/j.jssc.2024.124586
[12] C. Lai, J. Zhong, S. Huang, M. Li, Desalination and Water Treatment **315**, 32 (2023); https://doi.org/10.5004/dwt.2023.30088
[13] A. Helal, J. Yu, M. A. Ghanem, A. A. Labib, S. M. El-Sheikh, Journal of Molecular Structure **1312**(Pt. 2), 138553 (2024); https://doi.org/10.1016/j.molstruc.2024.138553

[14] M. Tanveer, A. R. Ali, M. A. Qadeer, M. Alam, H. H. Cheema, M. K. Hussain, M. H. Farooq, M. Shakil, F. Naseem, G. Nabi, Optical Materials **153**, 115555 (2024); https://doi.org/10.1016/j.optmat.2024.115555
[15] I. Ahmad, S. Shukrullah, M. Y. Naz, S. Ullah, M. A. Assiri, Journal of Industrial and Engineering Chemistry **105**, 1 (2024); https://doi.org/10.1016/j.jiec.2021.09.030
[16] H. Chawla, A. Chandra, P. P. Ingole, S. Garg, Journal of Industrial and Engineering Chemistry **95**, 1 (2024); https://doi.org/10.1016/j.jiec.2020.12.028
[17] Z. Cui, H. Yang, B. Wang, R. Li, X. Wang, Nanoscale Research Letters **11**, 190 (2016); https://doi.org/10.1186/s11671-016-1413-x